J. Fluid Mech. (1989), *vol.* 205, *pp.* 77–98
Printed in Great Britain

Liquid volume flux in a weak bubble plume

By A. M. LEITCH AND W. D. BAINES
Department of Mechanical Engineering, University of Toronto, Toronto, Ontario M5S 1A4, Canada

(Received 18 August 1987 and in revised form 21 December 1988)

A method has been devised for measuring the volume flux in a bubble plume in a homogeneous liquid. Laboratory experiments on weak bubble plumes using the method determined the flux as a function of height and gas flow rate for air flow rates between 0.41 and 6.25 cc/s. It was found that volume flux was proportional to the square-root of air flow and increased linearly with height. From measurement of bubble velocity it is concluded that the individual bubble wakes make an important contribution to the entrainment.

1. Introduction

Continuous injection of air from a source in a homogeneous liquid produces a stream of bubbles which entrains the liquid and carries it upward to the free surface, as sketched in figure 1. Near the source is a region of flow establishment, where the bubbles are accelerating and the plume structure changing rapidly. Above that is a highly turbulent region of 'established flow', and near the surface the entrained fluid is expelled in a radial current. The focus of this paper is on the established flow region.

Bubble plumes have been studied over a range of water depths from centimeters by Durst *et al.* (1986) to tens of meters by Milgram (1983). In this study the depth was about 0.5 m and the air flow was between 0.41 and 6.25 cm^3/s referenced to standard conditions. Both of these are small compared with the values used in the majority of reported studies of bubble plumes but these are typical of the weakest bubble plumes used in the chemical industries. Bubble plumes are used to mix fluids which are very hot or toxic, or which must be sealed from particular gases such as oxygen. In very hot liquids the flow velocities must be kept small to avoid high local heat transfer from the walls, and in other cases expensive gases such as argon are used to avoid oxidizing the liquid. In all cases the liquid volume flux has been the key property of interest. It is usually evaluated by measuring the velocity in the plume at a number of points and integrating over the cross-section. In addition to being time-consuming, this method suffers from inaccuracies because bubble plumes are subject to the lateral wandering noted by Baines & Hamilton (1959).

The present work describes a method of measurement of the liquid flux of a bubble plume which is adapted from the technique for the measurement of the volume flux in a turbulent buoyant plume described by Baines (1983). An interface between an upper stratified fluid and a lower homogeneous fluid is established in a closed container in which air bubbles are introduced from a source on the floor. The liquid flux in the plume at the level of the interface can be found by mass conservation from the movement of the interface. This principle is described more fully in §2. In §3 experiments that have utilized the technique, plus some others that measure additional properties of the plume, are described. In §4 the results are given, and in

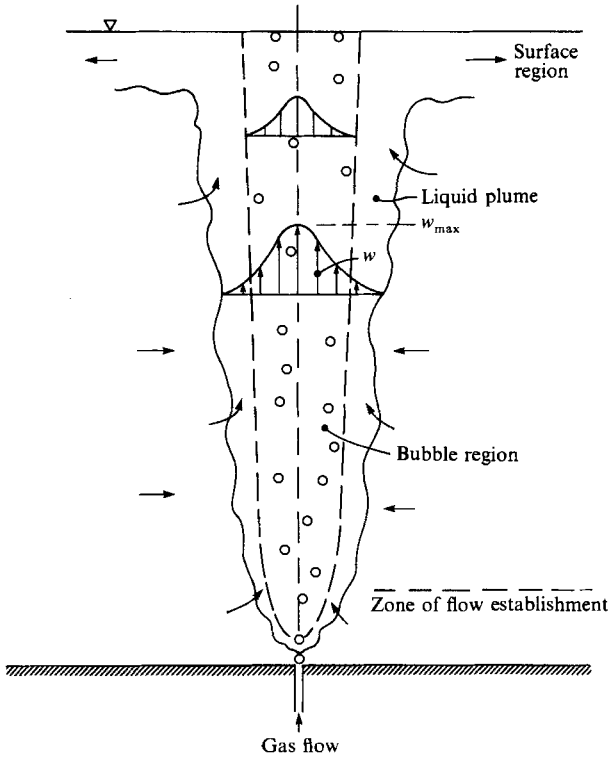

FIGURE 1. Schematic diagram of a bubble plume.

§5 the results and implications for the plume structure are discussed. Section 6 contains a comparison with other investigations, followed in the final section by the conclusions.

2. Principle of the technique

Consider a turbulent bubble plume in a stratified, confined fluid. The lower region is homogeneous and the upper is lighter and may contain a stable gradient. A weak interface z_i separates the two regions. The bubbles rising in the homogeneous region establish a shear flow which entrains environment fluid. Because of the relatively large momentum of this plume and the relatively weak density difference at the interface, the liquid flow is not deflected as a lateral current at the interface. It penetrates and, because of its turbulence, mixes with the lighter fluid it entrains from above the interface. All the plume fluid remains above z_i because it is less dense than the homogeneous fluid in the lower layer. This behaviour is evident in figure 2, which is a shadowgraph of a typical experiment. The interface z_i is the weaker lower interface. The stronger, upper interface is explained in the next section. How the mixed fluid is eventually distributed above z_i is not important, it is only important that traffic across the lower interface be one-way. Conservation of mass requires that the flux in the plume, Q_L is balanced by a downward motion of the interface.

$$Q_L(z_i) = -A\frac{dz_i}{dt}, \tag{1}$$

where A is the area of the tank and t time. This assumes that the area of the plume

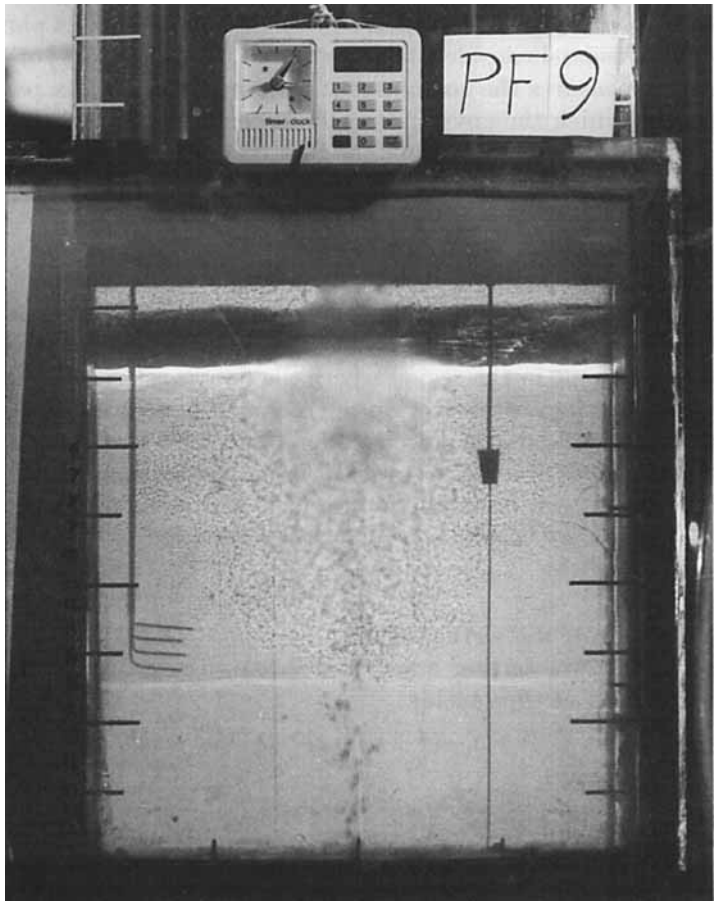

FIGURE 2. Bubble plume and interfaces shown in a shadowgraph taken during experimental PF9. Note the thick upper original interface and the thin lower interface which is used to determine $Q_L(z)$.

is negligible compared with A. The method of measuring Q_L involves recording z_i as a function of time to find the descent rate dz_i/dt. The procedure is similar to that used by Baines & Turner (1969) to determine the entrainment coefficient of a pure plume.

This method differs from the one used by Baines (1983) in the utilization of the interface velocity instead of the interface position. If a discharge $Q_L(z_i)$ is introduced into the lower layer the interface comes to rest at the elevation z_i. Attempts were made to use this second method in a few tests, but difficulties were encountered because the region above z_i contains a density gradient which becomes weaker with time. To obtain a true steady state, it would be necessary to introduce fresh fluid and extract brine evenly throughout the gradient, whereas our equipment allowed introduction and extraction of fluid only at specific levels. An additional problem was disturbance of the weak interface by the circulation due to the input. Results obtained showed reasonable agreement with those described below.

Inasmuch as the bubble plume is a free turbulent shear flow like a wake, plume or jet the volume flux probably follows a power law

$$Q_L = Bz^m, \tag{2}$$

where z is height above the source, and B and m are constants determined from experiment or derived from conservation equations. For a buoyant plume or jet from a point source dimensional considerations suffice to show that m is $\frac{5}{3}$ or 1 respectively. The parameter m measures the entrainment rate or volume influx per unit height – that is, the rate at which the environment fluid is engulfed. For $m > 1$, it increases with height and for $m = 1$ the entrainment rate is constant. If $0 < m < 1$ the inflow from the environment decreases with height and if $m < 0$ the flow is detraining. This cannot occur in a homogeneous environment since it requires infinite volume flux in the plume at $z = 0$.

There are similarities between a turbulent single-phase buoyant plume and a bubble plume. Both are driven by buoyancy and spread by the engulfing of quiescent environment fluid by turbulent eddies. It is reasonable to expect similar behaviour in the two types of plume in the region where the flow is established, although there cannot be an exact analogy. However, in the region of flow establishment the bubble plume is more complex and is not well understood. This is the region close to the source where the bubbles accelerate to the terminal velocity. For simplicity only the established flow region will be considered, and it will be assumed to originate at a 'virtual origin' which may be above or below the actual source. Thus the volume flux of the plume is defined by

$$Q_{\mathrm{L}} = B(z-z_0)^m \tag{3}$$

where z_0 is the height of the virtual origin.

Combining (1) and (3), setting $z = z_{\mathrm{i}}$ and integrating to give the height of the interface as a function of time yields

$$\zeta^{1-m} = 1-(1-m)\frac{B}{A}H^{m-1}t \quad (m \neq 1), \tag{4a}$$

$$\zeta = \mathrm{e}^{-\frac{B}{A}t} \quad (m = 1), \tag{4b}$$

where $\zeta = (z_{\mathrm{i}}-z_0)/H$ and $H+z_0$ is the height of the interface at $t = 0$. Numerical values of m, B and z_0 are derived in §4 by finding best fits for the measured values of z as a function of time.

3. Experiments

The experiments were performed in a square Perspex tank of side 40.5 cm and height 80 cm sketched in figure 3. The bubble nozzle was the end of a Teflon capillary tube with an internal diameter of 0.038 cm and a length of 15 cm which was set in a holder in the middle of the tank floor. The pressure fluctuations associated with bubbling were small compared with the drop through the capillary so the gas flow rate was constant. The tip of the nozzle was about 2 mm above the top of the holder, and the holder could be moved up and down relative to the floor of the tank. The nozzle was attached to a bottle of compressed nitrogen and the flow rate controlled by a regulator valve.

The eight experiments listed in table 1 were run with gas flow rates between 0.41 and 6.25 cc/s. These are small compared with 63 cc/s, the lowest flow rate used by Tacke *et al.* (1985), and very small compared with the gas flow rates of 200 to 59000 cc/s in the larger scale bubble plume experiments reported by Milgram (1983), so the flow is clearly in a different regime to other investigations. The liquid flux was measured over plume heights of 22 to 47 cm. In every case the submergence of the source was very small compared with the atmospheric head of 10.2 m so the effect of expansion of the bubbles has not been considered in the data presentation or

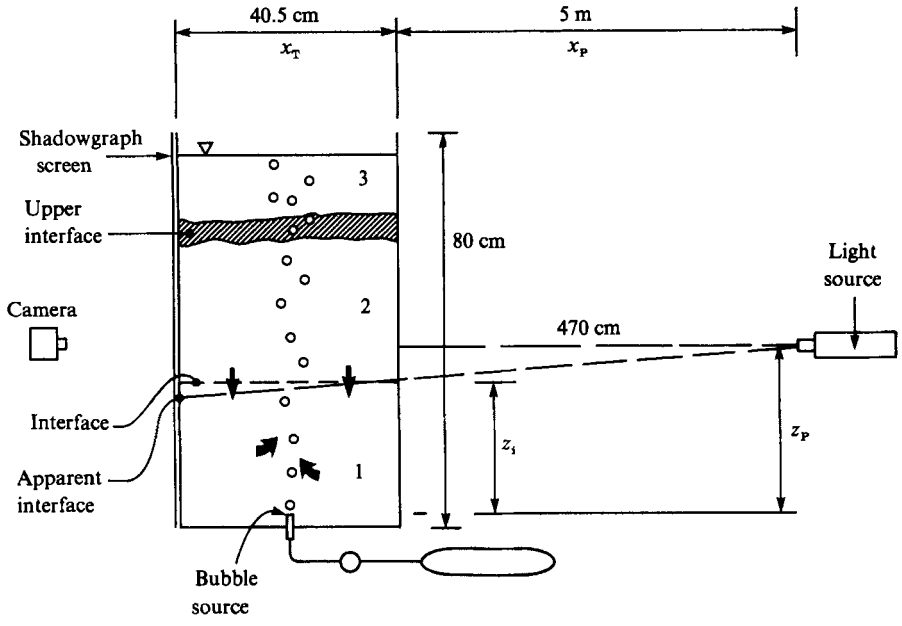

FIGURE 3. Sketch of experimental apparatus. Layer 1 is homogeneous and fresh, 2 is stratified and 3 is homogeneous and salty.

Experiment	Q_B(cc/s)	H(cm)	Run time (min)	ρ_S(g/cc)	$Re_B = \rho d_B w_S/\mu$	Eo	$\bar{d}_B$(cm)
PF16	6.25	47.0	11	1.08	850	2.5	0.42
PF9	3.30	30.5	13	1.08	1100	4.4	0.56
PF10	1.61	30.3	19	1.04	890	2.3	0.41
PF7	1.57	26.5	15	1.08	890	2.3	0.41
PF12	1.07	44.0	48	1.08	790	2.3	0.41
PF8	0.48	29.6	25	1.07	640	1.4	0.32
PF11	0.42	21.6	120	1.08	630	1.4	0.32
PF14	0.41	41.0	45	1.02	630	1.4	0.32

TABLE 1. Summary of experimental conditions, with $d_n = 0.038$ cm, $\rho = 1.02$—1.08 g/cc, $\mu = 1.05$–1.23×10^{-2} g/cm s, $\sigma = 74$–76 dynes/cm

analysis. The data were gathered over periods from 11 min to 2 h. The density of the brine was 1.08 g/cc, except for experiments PF10 and PF14, which were designed as a check on the possible influence of ρ_S, the density of the lower homogeneous layer.

The size of the bubbles is a function of the nozzle diameter d_n, the gas flow rate Q_B and the properties ρ, $\Delta\rho$, g, σ and μ (respectively the liquid density, density difference between liquid and gas, acceleration due to gravity, bubble–liquid surface tension and liquid viscosity) of the gas–liquid system; see table 1. As the flow rate increases, the average size of the bubbles increases and there is less uniformity of size. In these experiments the bubbles were seen to be of uniform size except at the highest gas flow rate. This can be seen in figure 4, which presents photographs of the plume at two air flow rates. In both figures the bubbles are uniformly sized, fairly evenly distributed and have the same lateral spread. In figure 4(*b*) the sizes are larger. Also evident is the liquid plume which was made visible by dye introduced near the

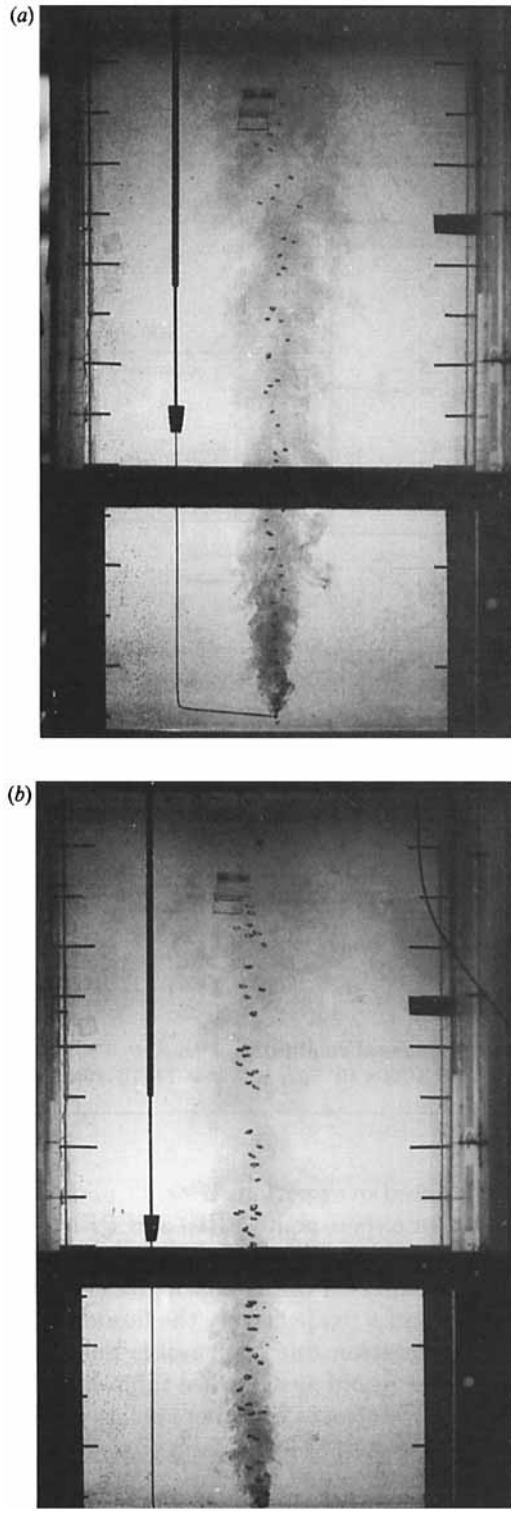

FIGURE 4. Photographs of bubble plumes in homogeneous environment. (a) $Q_B = 0.43$ cm^3/s, (b) $Q_B = 2.87$ cm^3/s.

source. There is not a large difference in the size and structure between the cases. In investigations with larger gas flow rates a wider distribution of bubble sizes was observed and the bubbles occupied more of the liquid plume cross-section.

The bubble sizes listed in table 1 were calculated from measured gas flow rate, bubble rise speed and number of bubbles present:

$$\bar{V}_B = \frac{Q_B}{N\bar{w}_B}, \tag{5}$$

where $\bar{V}_B$ = mean bubble volume (0.015–0.092 cc), N = mean number of bubbles per unit difference in elevation. These agree within 20% with those predicted in figure 12.1 of Clift, Grace & Weber (1978), except for the largest flow rate. This volume is predicted better by an empirical relation derived by Leibson *et al.* (1956)

$$\bar{d}_B = 0.29 d_n^{0.5} \mathrm{Re}_n^{0.33}. \tag{6}$$

Clift *et al.*'s book is not concerned with bubble interactions and the smaller observed bubble volume for $Q_B = 6.25$ is presumably due to breakup of larger bubbles by the turbulence in the plume. Estimates of bubble size from photographs agreed reasonably well with the calculations. It was observed in other experiments that the bubble size and lateral spread varied with the cleanliness of the source tube, but the bubbles did not change during the course of an experiment.

The shape, size and rise velocity of bubbles in liquids are related by dimensionless numbers expressing the relative importance of inertia, surface tension and viscosity. Figure 2.5 of Clift *et al.* (1978) gives the Reynolds number and shape of isolated bubbles as functions of the Eötvös number, $Eo = g\Delta\rho d_B^2/\sigma$, and the Morton number, $Mo = g\mu^4\Delta\rho/\rho^2\sigma^3$. For the present experiments Eo was between 1.2 and 4.4, and Mo was about 4×10^{-11}, and the figure predicts that the bubbles should be wobbling ellipsoids. This was confirmed by photographs. The predicted Reynolds numbers were in agreement with those given in table 1.

Additional useful information on the behaviour of single bubbles given in Clift *et al.* (1978) includes the ellipsicity (height-to-width ratio) as a function of Eo (their figure 7.8), and the drag coefficient as a function of Re (their figure 7.2). It is mentioned that between $Re = 565$ and 1510, bubbles rise in zigzag or helical paths as a result of vortex shedding in the wake. Surface-active impurities can prevent internal circulation, so that below Eo of about 4, bubbles behave more like rigid bodies (Harper 1972).

Before the start of an experiment the tank was filled to a depth of 40 to 60 cm with brine, usually with a concentration of 11 wt% ($\rho \approx 1.08$ g/cc). Fresh tap water was dribbled gently onto the top of the brine through a floating sponge, adding a further 20 cm to the total water depth. The interface region between the brine and fresh water was initially about 5 cm thick. This is the strong upper interface z_U seen in figure 2.

As the bubble flow started a second, lower interface z_i developed as sketched in figure 3. This is formed as a consequence of the liquid plume impinging on the layer of light fluid. The plume splits as it passes through z_U with a central core of liquid carried to the free surface where it is deflected and mixes uniformly with the lighter fluid. The outer zone of the plume has insufficient momentum for complete penetration of the interface and is deflected downwards and sideways, entraining some of the lighter fluid. The resulting mixed fluid comes to rest below z_U and its lower surface forms z_i.

As time proceeds the mixed outer-zone liquid continues to accumulate above z_i,

pushing this lower interface downwards. The plume does not split as it passes through z_i because of the very weak density step across it.

As the air flow was decreased or the initial density difference across z_U was increased, the intensity of z_i was reduced. After a certain point, a distinct lower interface did not form. The reason could be deduced from observing the outer-zone fluid impinging on z_U. If its momentum was too small there would be little entrainment of light fluid and the entrained fluid would not be completely mixed with the plume fluid. Thus there would not be a distinct layer of mixed fluid with a distinct lower surface. A criterion for the limit of formation of a lower interface can be devised by calculating a Froude number expressing the ratio of plume momentum to interface buoyant force:

$$Fr_i = \frac{w}{(g\,\Delta\rho/\rho\, b)^{\frac{1}{2}}}, \tag{7}$$

where b is the liquid plume radius. In these experiments it was found that if $Fr_i < 0.6$ a sharp lower interface did not form. Dyeing the upper-layer fluid allowed the mixed layer to be traced when the refractive index changes were too small to detect. For very low gas flow rates, the dye revealed large lateral variations in the position of the lower interface and an average height z_i was consequently very difficult to determine. To some extent it was possible to get around the limit for low air flows by using a large Q_B which produced a large liquid velocity w until z_i formed and then reducing the air flow. The outer-zone fluid can then cross the lower interface and mix with the stratified fluid as it rises and sinks in the weak gradient. However, the mixing of the plume fluid with the stratified fluid resulted in a very weak interface.

Flow visualization employed the shadowgraph technique. An interface is a region of rapidly changing refractive index, so light from a projector is bent downwards into the denser liquid leaving a dark shadow above a bright band. If the light source is level with the interface ($z_P = z_i$ in figure 3) then the top of the shadowed region marks the approximate position of the interface. If $z_P \neq z_i$, the interface position can be found from the apparent position z_a by

$$z_i - z_a = (z_P - z_a)\left[1 + n\frac{X_P}{X_T}\right]^{-1}, \tag{8}$$

where n (= 1.34–1.35 in our experiments) is the refractive index, X_T the length of the tank and X_P the distance of the light source from the tank. In these experiments, if the height z_P of the projector had not been varied then, as z_i changed by 25 cm, $z_i - z_a$ would vary by about 1.5 cm. This is much greater than the reading error in the interface position. The height of the interface was recorded on photographs taken at intervals of 10 s to 2 min.

Measurements were taken of the plume widths and the bubble rise velocities in a homogeneous liquid 70 cm deep to give additional information on the plume. Dye was injected slowly and continuously into the plume just above the nozzle for measurements of the width of the liquid plume. The dye was quickly distributed by turbulence and marked the outline of the plume as it rose. Fast shutter speed ($\leqslant 1/500$ s) photographs shown in figure 4(a, b) served the double purpose of revealing the outline of the liquid plume and the distribution of bubbles. Similar dyeing of jets and buoyant plumes by Baines (1975) had shown that the average position of the irregular edge marked a radius of 1.4b. It is reasonable to expect that a similar relationship might hold for the bubble-driven flow and that the visualization would allow us to compare the relative widths of the plume for different bubble flow

rates. The width of the bubble plume along the axis was also measured from the photographs.

Streak photographs of the bubbles were taken using shutter speeds of between 1/15 and 1/60 s when the plume was illuminated from the side through a slot. The light reflected off each bubble as a bright spot, the intensity of which was found to be largest at an angle of 135° from the line between the projector and the bubble plume. The length of the streaks gave the absolute rise velocity of the bubbles w_B.

4. Results

The data on the position of the interface z_i as a function of time were read from shadowgraph negatives and then fitted to a function of the form of equation (4*a*). m and z_0 were varied over the range 0.5 to 2 and 5 cm to -5 cm respectively. The best fit to the data was chosen as the one that gave the smallest r.m.s. error between measured and predicted z_i, rather than that for which the equation was best satisfied, since the equation becomes identically zero for $m = 1$. Generally there were a number of combinations of m and z_0 that gave good agreement, and the range of the results in table 2 reflects this. Outside the quoted range the fitted curve disagreed with the measurements of z_i by more than half a centimeter.

The clustering of the results around $m = 1$ is remarkable and consistent enough to conclude that the liquid flux Q_L does increase linearly above a virtual origin:

$$Q_L = Bz, \tag{9}$$

i.e.

$$\zeta = e^{-\frac{B}{A}t}$$

(equation (4*b*)). The uncertainty in the location of the virtual origin with respect to the nozzle tip is due both to the uncertainty in the best fit and to the finite size of the lower interface. In general the virtual origin is closer to the actual origin for higher values of Q_B. This is reasonable since for small Q_B the plume may be laminar at lower elevations. For bubble flow rates of 1 cc/s or less, the bubbles rose for about 2.5 cm in a steady spiral before spreading laterally and ascending more randomly.

Assuming that $m = 1$, optimum values for z_0 and B can be found by fitting the data to a function of the form of equation (4*b*). The data for four of the experiments are shown in figure 5 together with the calculated lines of best fit. Table 3 shows that the confidence limits on B and z_0 are small.

In figure 6 the parameter B is plotted as a function of the gas flow rate Q_B on a log scale. The results are well represented by the line

$$B = (5.0 \pm 0.15)\, Q_B^{0.5 \pm 0.05}, \tag{10}$$

and so we can summarize our results for the liquid flux in bubble plumes for gas flow rates between 0.41 and 6.25 Ncc/s and for heights of up to 47 cm by

$$Q_L = 5.0 Q_B^{\frac{1}{2}}(z - z_0). \tag{11}$$

In drawing the line in figure 6 more weight was given to the results at higher flow rates because the reading errors were less. Notice that, as is also indicated in tables 2 and 3, the data for PF10 follow exactly the same trend as the others, although a lower-density brine was used in this experiment. The density of the brine relative to water is only 4% lower so it is not surprising that the plume volume flux should be similar, but the density difference between the upper and lower interface has been reduced by a factor of two. This is a check on the technique.

Experiment	Q_B	m	z_0(cm)	B
PF16	6.25	0.95±0.1	0.25±0.15	14.3±4.1
PF9	3.30	1.0±0.1	0.1±0.2	8.9±2.2
PF10	1.61	0.95±0.1	0.5±0.3	7.5±1.0
PF7	1.57	1.0±0.1	0.7±0.5	6.3±2.0
PF12	1.07	1.0±0.1	0.5±0.3	5.4±1.5
PF8	0.48	1.05±0.1	1.3±0.4	3.3±0.9
PF11	0.42	1.05±0.1	0.8±0.2	3.1±0.6
PF14	0.41	1.05±0.1	1.3±0.4	3.6±1.0

TABLE 2. Best fits of m, z_0 and B to the data

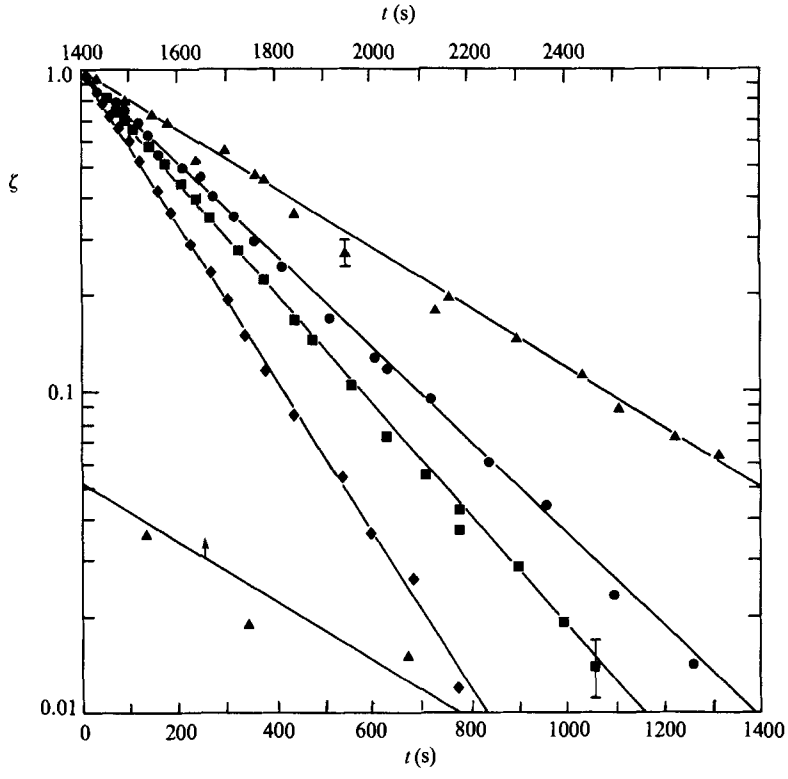

FIGURE 5. The normalized position of the interface z_i as a function of time for four experiments: ▲, $Q_B = 0.422$ cm^3/s; ●, $Q_B = 1.07$ cm^3/s; ■, $Q_B = 1.61$ cm^3/s; ◆, $Q_B = 3.30$ cm^3/s. The lines are best fits to the data, assuming the relation $\zeta = \exp(-(B/A)t)$.

The difference between average bubble velocities and slip velocity is shown in figure 7. The absolute velocities were calculated from streak photographs and their accuracy is limited by the precision of the camera shutter speed. Except in the first few centimeters above the nozzle where the streak lengths were difficult to measure there was no significant change in the bubble velocity with height and so the velocities are shown as a function of Q_B only. The slip velocity was determined from the terminal rise velocity of bubbles in stagnant tap water which was determined by Haberman & Morton (1954) as a function of bubble size. For the range of bubble sizes in the experiments the rise velocity is constant at about 23 cm/s. Goossens (1979)

Experiment	Q_B	z_0(cm)	B
PF16	6.25	0.25 ± 0.3	12.5 ± 0.4
PF9	3.30	-0.1 ± 0.3	9.1 ± 0.5
PF10	1.61	0.5 ± 0.3	6.4 ± 0.4
PF7	1.57	0.7 ± 0.3	6.3 ± 0.4
PF12	1.07	0.5 ± 0.3	5.4 ± 0.3
PF8	0.48	1.3 ± 0.3	4.1 ± 0.5
PF11	0.42	0.8 ± 0.3	3.5 ± 0.5
PF14	0.41	1.45 ± 0.3	4.2 ± 0.5

TABLE 3. Best fits for z_0 and B given $m = 1$

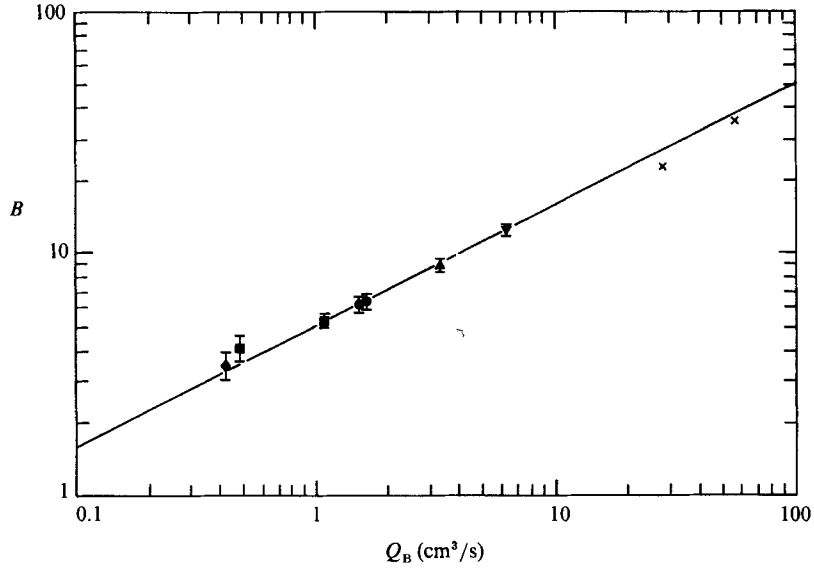

FIGURE 6. The parameter B defined as a function of bubble flow rate $Q_L = B(z-z_0)$. The line is the equation $B = 5Q_B^{\frac{1}{3}}$; ×, Goossens (1979). Other symbols defined in figure 5.

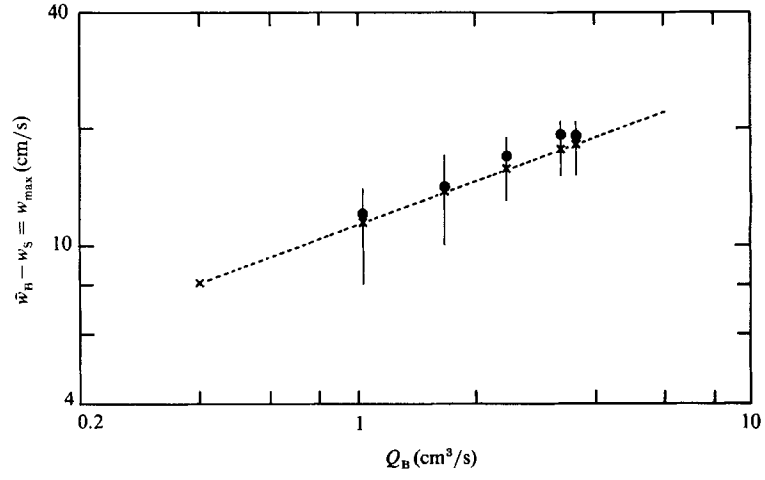

FIGURE 7. The difference between the mean bubble velocity and the slip velocity, $\bar{w}_B - w_S$ as a function of gas flow rate; ●, measured; ×, equation (20); ---, $w = 11.3Q_B^{0.37}$. Error bars denote spread of measured values.

mentions that the slip velocity of closely spaced bubbles is greater than it is in stagnant water owing to the interaction of the bubbles, and quotes a relation

$$w_S = w_{S\,stag}(1-\epsilon)^{-n}, \tag{12}$$

where n is between 2.4 and 3. In our experiments the void ratio ϵ (except very close to the nozzle) is only a few percent and so this effect was discounted. Since the bubbles are concentrated in the centre of the plume, $\bar{w}_B - w_S$ gives a measure of the maximum velocity in the liquid plume. This increased with Q_B. Note that the slip velocity was about twice the water velocity in every case. The line on figure 7 fits the formula

$$w = 11.3 Q_B^{0.37} \tag{13}$$

It is the best fit line to the crosses and will be explained in the next section.

Measurement of the width of the liquid plume was rendered difficult by plume wandering and for $Q_B < 1$ cc/s the intensity of turbulence was small and a distinct edge of the plume could not be seen. There appeared to be a slight increase with bubble flow rate, but overall the apparent visual width was given by

$$b_v = (0.4 \pm 0.1)\, z^{0.72 \pm 0.08}. \tag{14}$$

For bubble flow rates $\geqslant 6$ cc/s, the bubble plume spread approximately as the square-root of distance above the nozzle

$$b_c = 0.2 z^{\frac{1}{2}}. \tag{15a}$$

For lower flow rates the spread rate was less and depended on the size as well as the number of bubbles. Larger bubbles tended to diverge less than smaller ones and an approximate average was

$$b_c = (0.15 \pm 0.05)\, z^{\frac{1}{2}}. \tag{15b}$$

5. Implications for the plume structure

A comprehensive description of the dynamics of bubble plumes has not yet been given, as they share the complexity of other turbulent flows. The approach taken by investigators has generally been that of finding an empirical model to fit a limited range of experimental conditions. Below we outline a model for bubble plumes over the range of Q_B studied. For these weak plumes with low void ratio the analysis is focused on the liquid flow. The photographs in figure 4 of the dyed liquid plume show a turbulent flow with an appearance similar to a buoyant plume or jet. In this case the plume is driven by bubbles, which are moving faster than the liquid.

A bubble moving at constant velocity w_s relative to a liquid imposes a drag force equal to its buoyancy. Equating the drag force to the change in total momentum M of the liquid flow gives

$$\frac{dM}{dz} = \frac{\rho g Q_B}{w_B} \tag{16}$$

where w_B = the absolute velocity of a bubble. As noted above w_B was found to be constant along the plume so the right-hand side of (16) must be constant and the total momentum must increase linearly.

The photographs of figure 4 show that the bubbles are confined to a narrow plume about $\frac{1}{3}$ the diameter of the turbulent liquid plume. Also evident is the small volume of this bubble plume that is occupied by air. The mean void ratio ϵ calculated by counting the number of bubbles contained in a unit length of plume occupied by the bubbles and dividing the resulting volume by b_c gives $\epsilon \approx 0.1$ near the source and

$\epsilon \approx 0.013$ near the free surface. In the analyses of larger air flow plumes by Milgram (1983), Chesters, Doorn & Goossens (1980) and Goossens (1979) the void ratio distribution was treated like the density difference in a pure plume, that is, as a continuous variable. This approach was also taken by Durst *et al.* (1986) in the analysis of much sparser plumes.

Let us first evaluate the properties of the liquid plume assuming that the velocity profiles are similar as in a water jet or pure plume and ignoring the momentum and volume of the bubbles. A reasonable profile is the Gaussian distribution

$$w = w_{\mathrm{L}} \mathrm{e}^{-r^2/b^2}, \tag{17}$$

with characteristic radius b and maximum centreline velocity w_{L}. With this profile the liquid volume flux is

$$Q_{\mathrm{L}} = \pi w_{\mathrm{L}} b^2 \tag{18}$$

and the momentum is

$$M_{\mathrm{L}} = \tfrac{1}{2}\pi \rho w_{\mathrm{L}}^2 b^2. \tag{19}$$

Inserting M_{L} as the minimum value of M in (16) and substituting the result (11) in (18), produces a quadratic equation for the maximum value of w_{L} allowed by conservation of momentum. Its solution is

$$w_{\mathrm{L(max)}} = \tfrac{1}{2}\{-w_{\mathrm{s}} + [w_{\mathrm{s}}^2 + 1.6 g Q_{\mathrm{B}}^{\frac{1}{2}}]^{\frac{1}{2}}\}. \tag{20}$$

Example points are represented as crosses on figure 7. The line equation (13) is a fit to these points. Acknowledging the large uncertainties in the measurements of w_{B} and in the value of w_{s}, this result indicates that most of the momentum is associated with the mean flow rather than the turbulence.

Using (11) and the observation that w_{L} is independent of height above the source, (18) yields an expression for b:

$$b = 0.37 Q_{\mathrm{B}}^{0.065} (z - z_0)^{\frac{1}{2}}. \tag{21}$$

The discrepancy with (14) is not surprising in view of the wandering of the bubble column. The bubbles rise two or three times faster than the liquid velocity and in the time interval during which the outermost plume fluid rises to the top of the tank, the centre of the bubble column, which corresponds to the maximum of the liquid velocity, drifts around the liquid plume cross-section. This leads periodically to higher entrainment and lateral expansion at first one side of the plume and then the other. When averaged over time this results in a dyed visible plume which spreads more rapidly than if the bubble column were fixed at the centre, even if the instantaneous half-width may be represented by a square-root growth with height.

Although our measurements and the conservation laws provide a consistent model of the plume structure, they offer little insight into its dynamics. In describing the dynamics of single-phase jets, plumes and thermals, it is generally recognized that these flows increase their volume flux by the engulfing of surrounding fluid by large-scale eddies (Turner 1986). The entrainment hypothesis of Morton, Taylor & Turner (1956), which works well for single-phase flows, is that 'the mean inflow velocity across the edge of a turbulent flow is assumed to be proportional to a characteristic velocity, usually the local time-averaged maximum mean velocity or the mean velocity over the cross-section at the level of inflow' (Turner 1986). In a homogeneous environment this is equivalent to assuming dynamic similarity of the turbulent structure as well as the mean flow, so that the strength of the entraining eddies is directly related to the centreline velocity.

The entrainment assumption is used with the conservation equations for mass and

momentum to find the structure of the flow. For a Gaussian velocity distribution in a round plume, it gives

$$\frac{\mathrm{d}Q_{\mathrm{L}}}{\mathrm{d}z} = \alpha 2\pi b w_{\mathrm{L}}, \tag{22}$$

where α is the entrainment constant, which is 0.054 for jets and 0.083 for single phase plumes. Solution of (22) using (16), (18) and (19) yields

$$Q_{\mathrm{L}} = \left(\frac{2}{\pi}\frac{gQ_{\mathrm{B}}}{w_{\mathrm{B}}}\right)^{\frac{1}{2}} \tfrac{4}{5}\pi\alpha z^{\frac{5}{2}}, \quad b = \tfrac{4}{5}\pi^{\frac{1}{2}}\alpha z, \quad w_{\mathrm{L}} = \left(\frac{2}{\pi}\frac{gQ_{\mathrm{B}}}{w_{\mathrm{B}}}\right)^{\frac{1}{2}} \frac{3}{4\pi\alpha} z^{-\frac{1}{2}}. \tag{23}$$

The measurements discussed above show a square-root variation for Q_{L} with Q_{B}, and a plume radius b which is only very weakly dependent on Q_{B}; however, the more important relationships with elevation are not followed for any of the properties. This indicates that either the profiles are not similar or α is not constant. The bubble column wandering mentioned above would tend to produce a long time-averaged profile which is flatter at the centre and steeper at the edges than a Gaussian profile, and changes with height as the relative bubble displacement increases. This changing profile may contribute to the variation of the entrainment coefficient.

The idea that the entrainment assumption, in the simple form described by (22), is not appropriate to bubble plumes has been indicated before. Tacke *et al.* (1985) produce a figure showing the very diverse values of α calculated by different workers. Hussain & Narang (1983) weighted the velocities of liquid and bubbles to find a scaling velocity, but in our case α would still be a constant with height. Milgram (1983) calculated the entrainment coefficient for bubble plumes of various scales and correlated it with a 'bubble Froude number', which was a ratio of various local plume properties. This correlation does not, however, apply for our very weak plumes.

The concept of similarity of the mean and turbulent parts of the flow is not supported by consideration of the bubble plume structure, and in the remainder of this section we shall consider an alternative description of the plume. First, for completeness, we should take into account the added mass. In the flow establishment zone acceleration of the bubble involves the acceleration of a volume of water approximately one half of the bubble volume to the speed w_{s}. This is the 'added mass' contribution to the momentum of the flow (Clift *et al.* 1978).

The ratio of added-mass momentum to the increase in total momentum over a distance Δz is

$$\frac{M_{\mathrm{a}}}{\Delta M} = \frac{1}{2}\frac{w_{\mathrm{B}}^2}{g\Delta z}. \tag{24}$$

This ratio $\ll 1$ for $\Delta z \geqslant 10$ cm in all cases. For example, the largest observed value of w_{B} was about 42 cm/s so for $\Delta z = 10$ cm the rate of increase of momentum using (16) is 0.09. It is thus evident that the part of M transported by the added mass in the established flow zone is small. Most of M is associated with steadily rising liquid.

We now consider the flow produced by the steadily rising bubbles and the contribution to the plume of distinct bubble wakes and the background 'jet' flow.

The photos and measured velocities reveal a pattern of uniformly sized bubbles spaced 2 bubble diameters apart along the vertical and spread over a lateral area which increases from 1 to 5 bubble diameters in width. The slip velocity of 23 cm/s is from 1.5 to 3 times the absolute velocity of the steady but turbulent liquid flow. There should thus be a discernible wake for each bubble which spreads laterally at a small angle. In the upper parts of the plume the wakes should extend downstream

for at least 10 bubble diameters before intersecting another wake. After interaction with other wakes the individual flows should merge and become part of a flow which is steady relative to the source. We can thus separate the liquid plume into two regions. The inner region contains the bubbles and the flow consists of a collection of bubble wakes superposed on a constant background velocity. The wider outer region contains no bubbles and is a steady turbulent shear flow produced by the amalgamation of wakes which entrains liquid from the quiescent environment.

We can also consider the plume to have two components. The background flow in the inner region and the flow in the outer plume form a wide flow which is steady relative to the source. This is a mixing zone similar to a jet, except that momentum is continually supplied in the inner region by the wakes of the bubbles. The near wakes of the bubbles have large turbulent intensities, and mean velocity which is steady relative to the bubble but unsteady relative to the source. Figure 8 has been prepared to illustrate the magnitude of the steady and unsteady components for an elevation of 30 cm in a bubble plume driven by $Q_L = 1$ cm^3/s. The upper part of the figure shows the bubbles producing high-velocity wakes which merge into the background liquid jet flow, which is sketched in the lower part. The mean and turbulent velocities in the bubble wake have been scaled from the measurements of Uberoi & Freymuth (1970) who studied the wakes behind a solid sphere, and those for a liquid jet from the measurements of a pure jet made by Albertson *et al.* (1950). The comparison between a solid sphere and a bubble is reasonable since in even slightly contaminated water the no-slip condition applies at the surface of an air bubble (Clift *et al.* 1978). The main difference is that the ellipsicity of the bubble leads to an increased drag coefficient, if the Reynolds number is based on the diameter of an equivalent sphere.

The unsteady flow field in an individual bubble wake can be defined by considering the motion relative to the bubble. Buoyancy of the bubble is balanced by the drag and this must be equal to the momentum defect in the wake as discussed by Schlichting (1979):

$$D = \rho\pi \int_0^\infty u(w_s - u)\,\mathrm{d}(r^2) + \rho\pi \int_0^\infty (u')^2\,\mathrm{d}(r^2), \tag{25}$$

where u is the wake velocity relative to the background flow and r the radial distance from the centre of the plume. When u is small relative to w_s, and assuming that both mean and turbulent velocities follow similar profiles, it is readily shown that

$$u = \text{const} \times w_s (c_D d^2/x^2)^{\frac{1}{3}}; \quad b_1 = \text{const} \times (c_D d^2 x)^{\frac{1}{3}}, \tag{26}$$

where c_D is the drag coefficient, d the diameter of the sphere and b_1 the wake radius. It follows that the discharge and momentum in the wake relative to the background flow are

$$Q_w = \pi u b_1^2 = \text{const} \times w_s c_D d^2; \quad M_w = \tfrac{1}{2}\pi u^2 b_1^2 = \text{const} \times w_s^2 (c_D d^2)^{\frac{4}{3}} x^{-\frac{2}{3}}. \tag{27}$$

In this frame of reference, there is no entrainment into the wake and there is a loss of momentum. Relative to the bubble, Q increases with x and M is constant. The measurements of Uberoi & Freymuth (1970) confirm (26) for $x/d > 30$ and show that Q_w is constant (although the profile shape changes) for $19 < x/d$ at

$$Q_w = 0.041\pi w_s d^2. \tag{28}$$

Taking into account the greater drag of an ellipsoidal bubble relative to a sphere of the same volume, the drag would be larger by a factor of 4.5 ± 1 for the bubbles in our experiments.

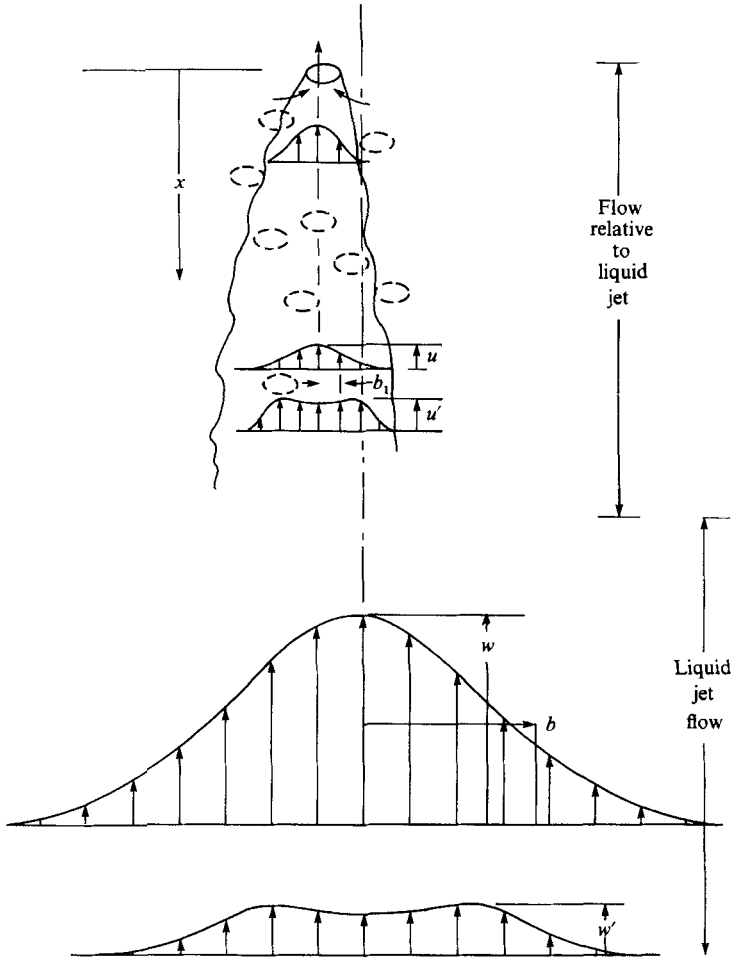

FIGURE 8. Sketch of distributions of mean velocity and turbulent intensity which probably exist in a plume at $z = 30$ cm driven by $Q_B = 1$ cm^3/s. Bubble wake velocities determined from measurements of wake of a sphere. Liquid jet velocities determined from measured Q_L and measurements in a free jet.

We can write the liquid volume flux due to the 'jet' and the wakes as

$$Q_L = \pi w_L b^2 + k\pi u b_1^2, \tag{29}$$

where k is the number of distinct wakes at a given level. Taking about one bubble per centimeter and assuming the wakes are distinct for about 10 bubble diameters gives $k \approx 4$. At mid-tank level ($z - z_0 = 20$ cm) the volume flux in each bubble wake is about 2% of the total liquid flux, so the discharge in the wakes is only about 8% of the total. It is instructive to compare the momentum of the two components. The total momentum flux for Gaussian mean velocity profiles is

$$M = \pi\rho(\tfrac{1}{2}w_L^2 b^2 + (w_L' b')^2 + \tfrac{1}{2}ku^2 b_1^2 + k(u'b_1')^2 + kw_L u b_1^2), \tag{30}$$
$$\text{(I)} \qquad \text{(II)} \qquad \text{(III)} \qquad \text{(IV)} \qquad \text{(V)}$$

where the terms and relative values at $z = 20$ are: (I) jet mean flow $\approx 89\%$ of total momentum; (II) jet turbulent flow $\approx 4\%$ of total; (III) sum of k wakes mean flow $\approx < 1\%$ of total. k has been taken as 4 for this calculation; (IV) sum of k wakes

Q_B(cc/s)	0.42	1.07	1.61	3.3	6.25
$\frac{dQ_L}{dz}\left[\frac{\text{theory}}{\text{measurement}}\right]$	0.26	0.34	0.43	0.48	0.64

TABLE 4. Ratios of fluxes: wake entrainment to plume entrainment

turbulent flow $\approx < 2\%$ of total; (V) interaction of k wakes and mean flow $\approx 5\%$ of total. Terms (I) and (II) increase linearly with z and the others are approximately constant along the plume so term (I) increases in importance with elevation. For example, at $z = 5$ cm in the above example term (I) is 72%. These figures are only approximate and vary between experiments, but they are consistent with our earlier observation that most of the momentum of these sparse bubble plumes is associated with the mean flow. In each bubble wake the turbulent component is about the same as the mean flow component, but distinct bubble wakes contribute relatively little to the total momentum.

While their momentum is small, bubble wakes are central to the dynamics of the plume; in particular, entrainment into the plume is linked to entrainment into the bubble wakes. Since the measurements of Uberoi & Freymuth (1970) show that Q_w is constant for $x/d > 19$ (the closest measurement that they made to the sphere) it is concluded that all of the entrainment to the wake of a moving bubble occurs in a short distance behind the bubble as sketched in figure 8. Thus, the central region of the flow is made up of moving sinks, one behind each bubble. At any instant, these sinks are entraining liquid from the outer region over short distances behind each bubble. The integration of all the entrainments is a uniform inflow along the length of the plume, the magnitude of which can be estimated from Q_w for a single bubble. If the entrainment occurs over a short length and the mean number of bubbles per centimeter is N then (from (28)) the inflow to all wakes is

$$\frac{dQ_L}{dz} = 0.041\left(\frac{c_D}{c_{D\,\text{sphere}}}\right)\pi w_s d_B^2 N$$

$$= 0.041\left(\frac{c_D}{c_{D\,\text{sphere}}}\right)6 w_s Q_B/d_B w_B. \tag{31}$$

The ratio of this entrainment flux to that observed for the plume (equation (11)) is given in table 4. It is seen that entrainment into the bubble wakes is a significant proportion of the entrainment into the liquid plume, and that the ratio increases with gas flow rate.

The near wakes of the bubbles are at the centre of the liquid plume whereas entrainment from the environment occurs at its boundary from larger scale eddies that are the product of the accumulated, interacting wakes. It is therefore reasonable that the entrainment flux into the plume is related, but not equal, to entrainment into the near wakes. For the smallest gas flow rates in our experiments, the liquid 'jet' entrained four times as much from the environment as the wakes did from the jet, whereas for the largest gas flow rate the jet entrained less than twice as much as the wakes. This difference may be due to the more widely spaced bubbles (relative to bubble size) in the weaker flows creating relatively larger entraining eddies.

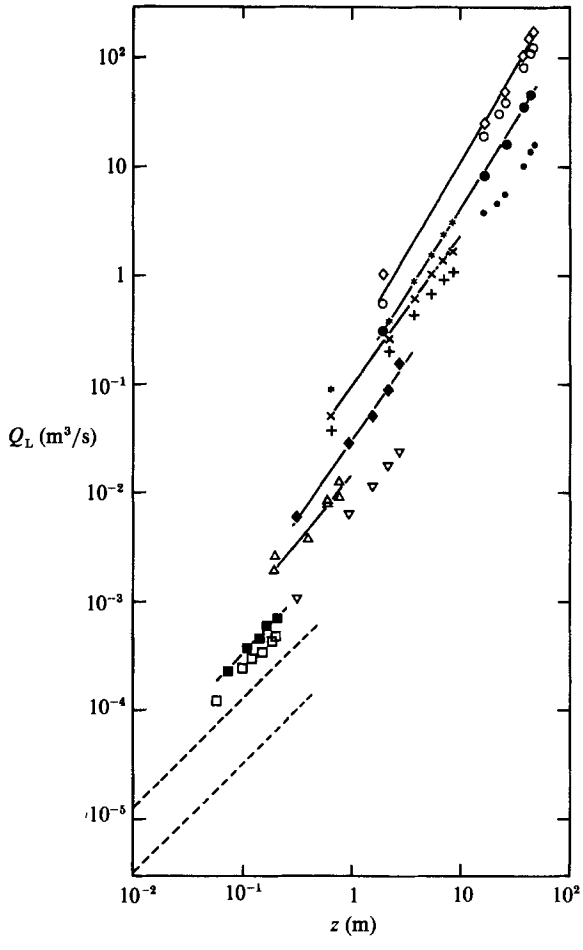

FIGURE 9. The liquid volume flux as a function of height for a range of gas glow rates Q_0 at the nozzle (SI units). The sources of the data and the submergence depth of the nozzle are:

		H (cm)	Q_0 (m³/s)
Present work	---	40	$0.41–6.3 \times 10^{-6}$
Goossens (1979)	□	28	2.8×10^{-5}
	■	28	5.6×10^{-5}
Tekeli & Maxwell (1980)	△	100	1.29×10^{-4}
Milgrm & Van Houten (1982)	▽	3660	1.55×10^{-4}
	●	3660	1.72×10^{-3}
Fannelop & Sjoen (1974)	+	1000	2.53×10^{-3}
	×	1000	5.05×10^{-3}
	*	1000	1.01×10^{-2}
Milgram (1983)	•	5000	4.07×10^{-3}
	●	5000	2×10^{-2}
	○	5000	4.8×10^{-2}
	◇	5000	0.1

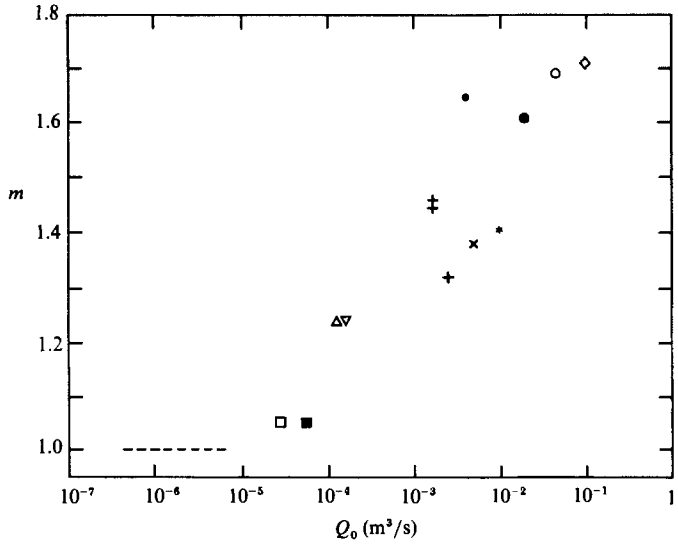

FIGURE 10. The exponent m as a function of Q_0 for the data in figure 9, assuming power-law growth of the liquid volume flux Q_L. Symbols are defined in figure 9.

6. Comparison with other investigations

It is instructive to compare these measurements to those reported in the literature for a wide range of conditions. The data available cover water depths up to two orders of magnitude, and normalized gas flow rates up to six orders of magnitude, greater than the values reported above. All of these are plotted on figure 9 as the liquid volume flux as a function of elevation above the source. It is evident that there is a smooth progression in flux as either the elevation or the air flow is increased. The various sets of points are identified by the air flow Q_0 in m^3/s as the nozzle. This contrasts to the usual comparison of flow at atmospheric pressure but it is used to account in a crude way for the second parameter which affects the plume development. As the bubbles rise the volume expands because of the reduction in static pressure. The change is small for nozzle submergence of less than a meter but is a factor in all of the larger scale experiments. An empirical correction scheme could be employed as was done by Tekeli & Maxwell (1980) but this does not appear to be worth the effort.

Note first that the empirical power-law increase in Q_L with height holds remarkably well over the entire range of conditions, and second that the steepness of the lines increases systematically with Q_0 and H. The power law $m = 1$ obtained for our experiments is consistent with the trend of the data for larger scale plumes. figure 10 is a plot of the slope m with gas flow rate Q_0. The symbols indicate the height dependence. It is interesting to note that the slope is of the order 3/2 for large scales and that this is the value for similarity and a constant entrainment coefficient.

It is physically reasonable that the liquid volume flux should increase more rapidly in deeper water because the size of the bubbles and hence their buoyancy then increases significantly. An increase with gas flow rate might be accounted for by the fact that at higher gas flow rates the high void fraction near the nozzle means that there is not much liquid between the bubbles. As the bubble cloud spreads out more liquid is entrained. There is some uncertainty in the value of m for each line, because it depends on how much weight and reliance is put on the data point at the lowest

elevation. The clustering of the points suggests that the submergence depth is more important than the gas flow rate in determining m.

Tacke *et al.* (1985) took a series of very careful measurements of ϵ as a function of r and z for a range of Q_B and solved the momentum equations to find a best value of constant α for their data. However, their measurements of ϵ_{max} and b_ϵ, when put together with their other assumptions, are consistent with a constant value of α. According to their data, α decreases by a factor of 2 to 2.6 over the height of their reservoir between 5 and 40 cm. It is evident in this case also that the entrainment coefficient does not scale simply with the maximum liquid velocity.

Milgram (1983) and Goossens (1979) both point out that the momentum equation should include the contribution of turbulent fluctuations to the momentum flux. They found in some cases only a half to three-quarters of the momentum flux was carried by the mean momentum. Milgram introduced a 'momentum amplification factor' γ, which is the total momentum divided by the momentum carried by the mean flow. Milgram (1983) found a correlation of his measured γ with a dimensionless number that he called the 'phase distribution number', but it is not applicable at the low gas flow rates of the present work, since it predicts γ values of several hundred. He also found $\gamma < 1$ at large gas flow rates and this requires that the turbulent momentum be negative. This is impossible so there must be other factors in the flow. One of these is the momentum carried by the unsteady flow in the wakes. This would appear as turbulence if measurements were made of the mean and fluctuating velocities using a standard technique.

7. Conclusions

A method is outlined by which the liquid flux is carried by a bubble plume can be measured as a function of elevation. The method involves observations of a moving interface created by the plume in a stratified, confined environment. There are practical limits on the scale of the plume that can be studied in the laboratory but the method could be applied in many field studies. For example, if Bugg Spring contained a density stratification, at Milgram's (1983) largest gas flow rate the interface would traverse a depth of 37 m in about an hour and a half. The lower limit of plume size is dictated by the plume being turbulent, since for laminar plumes a sharp interface does not form.

The method was used to find the liquid flux as a function of elevation and gas flow rate for a bubble plume from a single nozzle for gas flow rates between 0.41 and 6.25 cc/s and over a height of about 40 cm. It was found that (equation (11))

$$Q_L = 5.0 Q_B^{\frac{1}{3}}(z - z_0).$$

Other observations of the plume structure revealed that the maximum liquid velocity in the plume was approximately constant over the height range at (equation (13))

$$w_L = 11.3 Q_B^{0.37},$$

the bubble plume spread as the square-root of height (equation (15*b*))

$$b_\epsilon = 0.15 \pm 0.05 z^{\frac{1}{2}}.$$

Dying the liquid plume did not give a realistic estimate of its shape because of plume wandering. The linear growth of Q_L and the constancy of w_L with z together imply the square-root growth of the plume width. Calculations indicate that most of the

momentum is associated with the mean flow rather than the turbulence of the liquid plume, hence the width is approximately (equation (21))

$$b = 0.37 Q_B^{0.065} (z - z_0)^{\frac{1}{2}}.$$

The ratio of width of bubble region to width of turbulent region is 0.4 ± 0.15. The equivalent density/velocity width ratio of a pure plume is of order unity.

The entrainment assumption of Morton *et al.* (1956) in its simplest form (equation (22)) is not appropriate to these bubble plumes: it predicts a liquid volume flux which increases as $z^{\frac{3}{2}}$ (equation (23)). Thus the entraining eddies at the edge of the flow do not scale simply with the centreline liquid velocity. An alternative model, where entrainment into the plume is controlled by entrainment into the near wakes of the individual bubbles, gives the correct linear variation of the liquid flux with height. The magnitude of near-wake entrainment is less than that of the plume, since the bubbles entrain from the liquid plume rather than directly from the environment.

It is not expected that these features of the plume structure will necessarily hold for plumes of larger scales than those studied, since they may rest on the bubbles preserving distinct wakes for several diameters. However, the liquid volume flux of plumes orders of magnitude larger does increase with height approximately according to a power law, with the exponent increasing with nozzle submergence and gas flow rate at the nozzle as shown in figure 10. Equation (11) is consistent with the trend of the other data.

This study was supported by the Natural Sciences and Engineering Research Council of Canada under grant A-1066. The first author was in receipt of a postdoctoral fellowship covered by the grant for the duration of the study. This support is gratefully acknowledged by the authors. The apparatus was constructed by Mr Ernesto Morala who also assisted with some of the experiments. His care and concern are sincerely appreciated.

REFERENCES

ALBERTSON, M. L., DAI, Y-B., JENSEN, R. A. & ROUSE, H. 1950 Diffusion of submerged jets. *Trans. ASCE* **115**, 639–697.

BAINES, W. D. 1975 Entrainment by a plume or jet at a density interface. *J. Fluid Mech.* **68**, 309–320.

BAINES, W. D. 1983 A technique for the direct measurement of volume flux of a plume. *J. Fluid Mech.* **132**, 247–256.

BAINES, W. D. & HAMILTON, G. F. 1959 On the flow of water induced by a rising column of air bubbles. *Intl Assoc. for Hydraulic Research, 8th Congr., Montreal, 24–29 August*, pp. 7D1–7D17.

BAINES, W. D. & TURNER, J. S. 1969 Turbulent buoyant convection from a source in a confined region. *J. Fluid Mech.* **37**, 51–80.

CHESTERS, A. K., DOORN, M. VAN & GOOSSENS L. H. J. 1980 A general model for unconfined bubble plumes from extended sources. *Intl J. Multiphase Flow* **6**, 499–521.

CLIFT, R., GRACE, J. R. & WEBER, M. E. 1978 *Bubbles, Drops and Particles*, Academic.

DURST, F., SCHOENUNG, B., SELANGER, K. & WINTER, M. 1986 Bubble-driven liquid flows. *J. Fluid Mech.* **170**, 53–82.

FANNELOP, T. K. & SJOEN, K. 1974 Hydrodynamics of underwater blowouts. *Proc. Coastal Engng Conf.*, pp. 2209–2226.

GOOSSENS, L. H. J. 1979 Reservoir destratification with bubble columns. Ph.D. Thesis, Delft University of Technology.

HABERMAN, W. L. & MORTON, R. K. 1954 An experimental study of bubbles moving in liquids. *ASCE Proc.* **80**, 387.

HARPER, J. F. 1972 The motion of bubbles and drops through liquids. *Adv. Appl. Mech.* **12**, 59–129.

HUSSAIN, N. A. & NARANG, B. S. 1983 Simplified analysis of air-bubbles in moderately stratified environments. *Trans. ASME* C: *J. Heat Transfer* **106**, 543–551.

LEIBSON, I., HOLCOMB, E. J., CACOSO, A. G. & JAMIC, J. J. 1956 Rate of flow and mechanics of bubble formation from single submerged orifices. *AIChE J.* **2**, 296–306.

MILGRAM, J. H. 1983 Mean flow in round bubble plumes. *J. Fluid Mech.* **133**, 345–376.

MILGRAM, J. H. & VAN HOUTEN, R. J. 1982 Plumes from sub-sea well blowouts. *Proc. 3rd Intl Conf.. BOSS*, vol. 1, pp. 659–684.

MORTON, B. R., TAYLOR, G. I. & TURNER, J. S. 1956 Turbulent gravitational convection from maintained and instantaneous sources. *Proc. R. Soc. Lond.* A **234**, 1–23.

SCHLICHTING, H. 1979 *Boundary Layer Theory*. McGraw-Hill.

TACKE, K. H., SCHUBERT, H. G., WEBER, D. J. & SCHWERDTFEGER, K. 1985 Characteristics of round vertical gas bubble jets. *Metall. Trans.* **16B**, 263–275.

TEKELI, S. & MAXWELL, W. H. C. 1980 Physical modelling of bubble screens. *Proc. ASCE* **106** (WW1), 49–64.

TURNER, J. S. 1986 Turbulent entrainment: the development of the entrainment assumption, and its application to geophysical flows. *J. Fluid Mech.* **173**, 431–471.

UBEROI, M. S. & FREYMUTH, P. 1970 Turbulent energy balance and spectra of the axisymmetric wake. *Phys. Fluids* **12**, 2205–2210.